Proceedings of the 16th International Conference on Soil Mechanics and Geotechnical Engineering

doi:10.3233/978-1-61499-656-9-909

Numerical analysis of localized deformations in clay specimens using subloading t_{ij} model

Analyses numériques de déformations locales de spécimens d'argile avec l'utilisation du "subloading t_{ij} model"

M. Hinokio & T. Nakai
Department of Civil Engineering Nagoya Institute of Technology, Japan

M. Miyata
Wakayama Prefectural office, Japan

ABSTRACT
Finite element analyses based on infinitesimal deformation and finite deformation theories are carried out to investigate the mechanism of the localized deformation of normally and over consolidated clays in drained shear tests. For this purpose, an isotropic hardening elastoplastic model for soils, named subloading tij-model, is used in the analysis. Two different geometrical conditions are assumed. - plane strain condition (2D) and triaxial condition (3D). The developments of shear bands in clays in these conditions are well simulated by the present finite element analyses.

RÉSUMÉ
Des analyses numériques par éléments finis basées sur les théories de déformations infinitésimales et déformations finies ont été réalisées afin d'étudier le mécanisme de déformations locales d'argiles normalement consolidées et surconsolidées en essai de cisaillement drainé. A cette fin, est utilisé un modèle isotropique de comportement élastoplastique pour les sols, appelé le "subloading tij model". Deux conditions géométriques distinctes sont modélisées, la condition de contrainte plane (2D) et la condition triaxiale (3D). Les développements des bandes de cisaillement des argiles dans ces conditions sont ainsi simulés lors de ces analyses par éléments finis.

1 INTRODUCTION

Localization of deformation is usually considered as a boundary value problem in numerical analyses. On the other hand, triaxial tests, plane strain tests and other laboratory tests are generally simulated as a local problem, integrating the stress-strain relation at a single point. This is the same as to consider that deformations occur homogeneously over a finite element and will be referred as the *ideal* test. In actual conditions, however, heterogeneous deformations occur in a sample as shear deformation develops; and consequently localization of deformations should be considered as a form of shear band. In this paper, shear band is simulated numerically by finite element analyses, considering localization of deformation as a boundary value problem. In many researches, finite element simulations based on finite deformation theory have been used to reproduce shear bands numerically using soil-water coupled analyses (Yatomi et al., 1989, Asaoka & Noda, 1995, Asaoka et al., 1997, Oka et al., 1995). Nevertheless, it is possible to simulate localization using drained analysis. Hinokio et al. (2002) carried out such type of analysis for confined shear tests under 2D condition, considering just one quarter of the specimen due to the double symmetry of the problem. Here, analyses are performed for the whole section under both 2D and 3D conditions.

2 OUTLINE OF SUBLOADING TIJ MODEL

An elastoplastic constitutive model for soils, named subloading t_{ij}-model (Nakai & Hinokio, 2004), is used in finite element analyses in this paper. This model requires only a few unified material parameters, but can describe properly the following typical characteristics of soils: (1) influence of intermediate principal stress on the deformation and strength of clay; (2) influence of stress path on the direction of plastic flow. These features could also be simulated with t_{ij}-clay model (Nakai & Matsuoka, 1986), but subloading t_{ij}-model adds the following aspect: (3) influence of density and/or confining pressure.

Table 1. Comparison of tensors and scalars related to stress and strain increment between ordinary concept and t_{ij}-concept.

ordinary concept	t_{ij} concept
σ_{ij}	$t_{ij}=\sigma_{ik}a_{kj}$
δ_{ij} (*unit tensor*)	a_{ij}
$p=\sigma_{ij}\delta_{ij}/3$	$t_N=t_{ij}a_{ij}$
$s_{ij}=\sigma_{ij}-p\delta_{ij}$	$t'_{ij}=t_{ij}-t_N a_{ij}$
$q=\sqrt{(3/2)s_{ij}s_{ij}}$	$t_S=\sqrt{t'_{ij}t'_{ij}}$
$\eta_{ij}=s_{ij}/p$	$x_{ij}=t'_{ij}/t_N$
$\eta=q/p=\sqrt{(3/2)\eta_{ij}\eta_{ij}}$	$X=t_S/t_N=\sqrt{x_{ij}x_{ij}}$
$\eta_{ij}^*=(s_{ij}-s_{ij0})/p$	$x_{ij}^*=x_{ij}-n_{ij}$
$\eta^*=\sqrt{(3/2)\eta_{ij}^*\eta_{ij}^*}$	$X=\sqrt{x_{ij}^*x_{ij}^*}$
$d\varepsilon_v=d\varepsilon_{ij}\delta_{ij}$	$d\varepsilon_{SMP}^*=d\varepsilon_{ij}a_{ij}$
$de_{ij}=d\varepsilon_{ij}-d\varepsilon_v\delta_{ij}/3$	$d\varepsilon'_{ij}=d\varepsilon_{ij}-d\varepsilon_{SMP}^*a_{ij}$
$d\varepsilon_d=\sqrt{(2/3)de_{ij}de_{ij}}$	$d\gamma_{SMP}^*=\sqrt{d\varepsilon'_{ij}d\varepsilon'_{ij}}$

$$a_{ij}=\sqrt{\frac{I_3}{I_2}}\cdot r_{ij}^{-1},\quad r_{ik}r_{kj}=\sigma_{ij}$$

(I_2 and I_3 : 2nd and 3rd stress invariants)

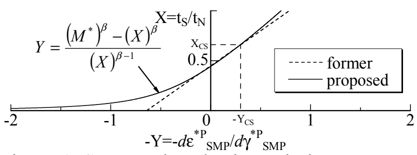

Figure 1. Stress ratio- plastic strain increment ratio relation of the proposed model.

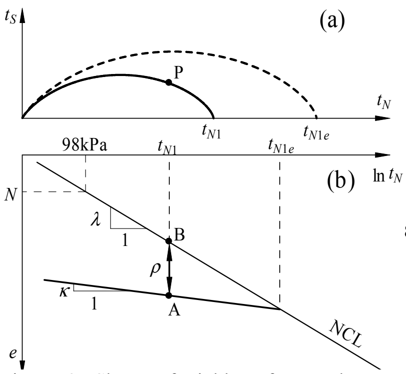

Figure 2. Shape of yield surface and normally yield surface, and definition of ρ.

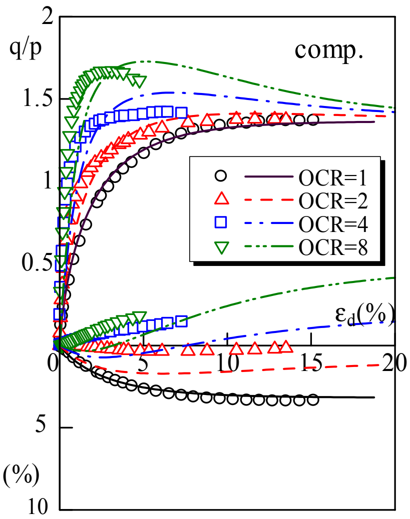

Figure 3. Observed and calculated results of triaxial compression tests with different over consolidation ratio.

Table 1 shows a comparison between the stress and strain increment tensors and scalar quantities used in conventional models and those used in models adopting the t_{ij}-concept. Assuming an associate flow rule in t_{ij} space, and using the relation between stress ratio and plastic strain increment ratio shown as the solid line in Figure 1, the following expression can be deduced for the yield function:

$$f = \ln t_N + \varsigma_{(X)} - \ln t_{N1} = 0\,, \qquad \varsigma_{(X)} = \frac{1}{\beta}\left(\frac{X}{M^*}\right)^{\beta} \tag{1}$$

The plastic strain increment is split into a component obeying an associate flow $d\varepsilon_{ij}^{p(AF)}$, and an isotropic compression component $d\varepsilon_{ij}^{p(IC)}$, as shown in the following equation:

$$d\varepsilon_{ij}^{p} = d\varepsilon_{ij}^{p(AF)} + d\varepsilon_{ij}^{p(IC)} \tag{2}$$

Using the subloading concept by Hashiguchi (1980), it is possible to consider the influence of density and/or confining pressure and the yield function can be expressed as follows:

$$\begin{aligned} f &= \ln\frac{t_N}{t_{N0}} + \varsigma_{(X)} - \left(\ln\frac{t_{N1e}}{t_{N0}} - \ln\frac{t_{N1e}}{t_{N1}}\right) \\ &= \ln\frac{t_N}{t_{N0}} + \varsigma_{(X)} - \left(\frac{1+e_0}{\lambda-\kappa}\varepsilon_v^p - \frac{\rho}{\lambda-\kappa}\right) = 0 \end{aligned} \tag{3}$$

Here, as shown in Figure 2, t_{N1} measures the size of the yield surface passing through the present stress, and t_{N1e} measures the size of the normal surface, which is related to the present plastic volumetric strain (or void ratio). For a reference isotropic stress condition (t_N=t_{N0}, X=0), ε_v^p is zero at the difference of the void ratios ρ between A and B can be regarded as an index of soil density. The strain increment obtained from Eqs. (2) and (3) and the consistency condition df=0.

$$d\varepsilon_{ij}^{p(AF)} = \Lambda\frac{\partial f}{\partial t_{ij}}\,, \Lambda = \frac{df_\sigma - \frac{1}{C_p}K_{NC}\langle dt_N\rangle}{h^p} = \frac{df_\sigma - \frac{1}{C_p}K_{NC}\langle dt_N\rangle}{\frac{1}{C_p}\left(\frac{\partial f}{\partial t_{ii}} + \frac{G(\rho)}{t_N}\right)} \tag{4}$$

$$d\varepsilon_{ij}^{p(IC)} = \frac{a_{ii}}{a_{ii} + G(\rho)}\cdot K_{NC}\langle dt_N\rangle\frac{\delta_{ij}}{3} \tag{5}$$

$$K_{NC} = C_p\frac{1}{t_N}\cdot\frac{t_N}{t_{N1}} = C_p\frac{1}{t_N}\cdot\exp\{-\varsigma_{(X)}\} \tag{6}$$

where $G(\rho)$ is a monotonically increasing function, which satisfies the condition $G(0)$=0. Nakai & Hinokio (2004) assume the following equation, in which a is a material parameter:

$$G(\rho) = a\cdot\rho^2 \qquad (a:\ \textit{material parameter}\,) \tag{7}$$

Figure 3 shows the results and ideal simulations of triaxial compression tests on Fujinomori clays with different over consolidation ratios (OCR=1, 2, 4 and 8). The present model describes well the deformation and strength of normally consolidated clay and can also predict well the influence of over consolidation ratio on the deformation, dilatancy and strength of clays. The values of material parameters of Fujinomori Clay used in the analyses are presented in Table 2.

Table 2. Values of material parameters for Fujinomori clay.

C_t=λ/(1+e_0)	5.08×10^{-2}
C_e=κ/(1+e_0)	1.12×10^{-2}
N=e_{NC} *at p=98kPa & q=0kPa*	0.83
R_{CS}=$(\sigma_1/\sigma_3)_{CS(comp.)}$	3.5
a	500
β	1.5
ν	0.2

3 METHODS OF ANALYSES

In this research, analyses are carried out for drained compression tests under plane strain (2D) and triaxial (3D) conditions for both normally consolidated clay and over consolidated clay (OCR=10). Analyses based on infinitesimal deformation theory and finite deformation theory as well were performed. Moreover, three-dimension finite element analyses were also performed to compare with the results obtained under plane strain conditions.

Figure 4 shows the finite element meshes used in these analyses. A rectangular specimen with a height of 10cm and a width of 5cm (and a depth of 5cm in triaxial condition) is considered. Figure 4(a) shows the mesh for plane strain condition consisting of 800 elements (20 elements in width and 40 in height). In triaxial conditions, the mesh consists of 2000 elements (20 in height, 10 in width and 10 in depth). As for the boundary conditions, the lateral faces are free to displace and have constant imposed stresses, the bottom face is kept perfectly fixed, and the top face is movable in the horizontal direction (in triaxial condition, horizontal movement is kept free in the x-direction). Vertical displacements are applied at the top face of the specimen to simulate loading, until a total axial strain of 20%. The initial stress state is isotropic with p_0=196kPa for all elements.

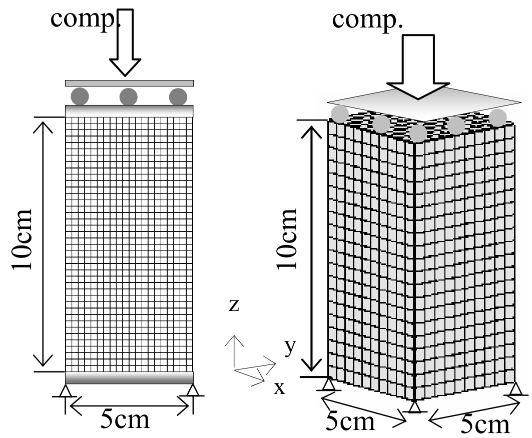

a) plane strain condition　　b) triaxial condition

Figure 4. Finite element mesh.

4 RESULTS AND DISCUSSIONS

The *average* behavior of the specimen is shown in Figure 5 (NC clay) and Figure 6 (OC clay) for plane strain condition. The solid line shows the analytical solution for a single point, obtained integrating the stress-strain relation for given imposed strain increments (henceforth-forward, called *ideal* behavior). In this paper, the upper bar(-) sign with stress, strain and void ratio is used to indicate the *average* result in the specimen as a mass. The average axial stress is obtained by dividing the total vertical force, computed from the nodal reactions at the top face, by the cross-sectional area of the sample. The void ratio as a mass is the average value of the void ratios of all elements in the specimen. From these figures, it can be seen that the average stress-strain behavior is the same as the ideal behavior in the early stages of shearing. However, after reaching peak strength the average deviator stress departs from the ideal behavior, and either decreases or becomes constant. In all cases, the average peak deviator stress occurred in for smaller strains and reached lower values than those compute for the ideal curve. With

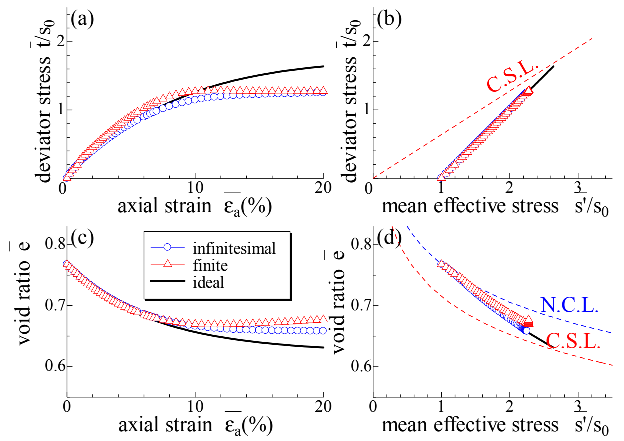

Figure 5. Calculated stress-strain relations as a mass –2D (OCR=1).

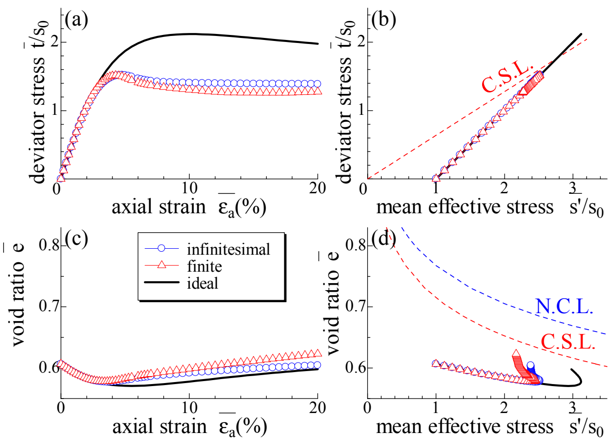

Figure 6. Calculated stress-strain relations as a mass –2D (OCR=10).

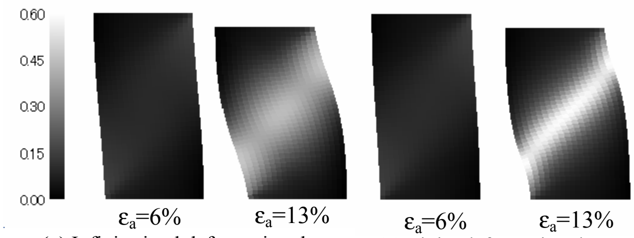

(a) Infinitesimal deformation theory **(b)** Finite deformation theory

Figure 7. Distributions of deviator strain –2D (OCR=1).

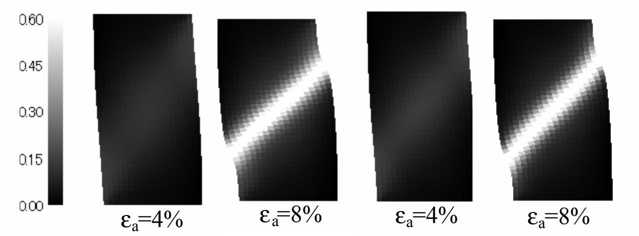

(a) Infinitesimal deformation theory **(b)** Finite deformation theory

Figure 8 Distributions of deviator strain –2D(OCR=10).

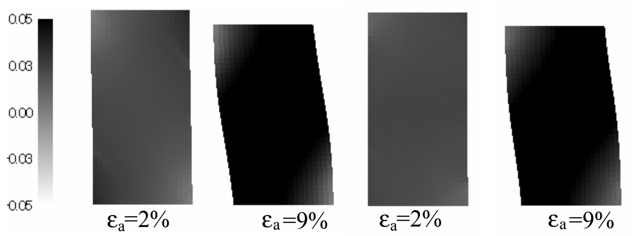

(a) Infinitesimal deformation theory **(b)** Finite deformation theory

Figure 9. Distributions of volumetric strain –2D (OCR=1).

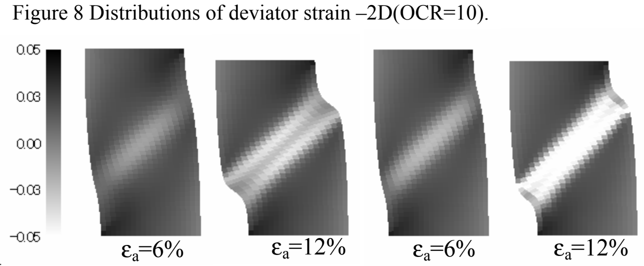

(a) Infinitesimal deformation theory **(b)** Finite deformation theory

Figure 10. Distributions of volumetric strain –2D(OCR=10).

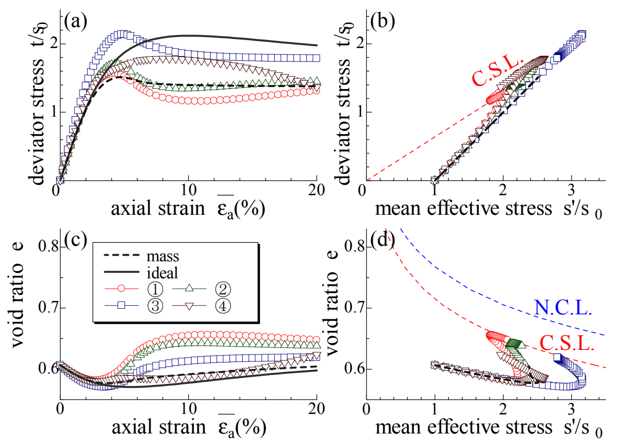

Figure 11. Stress- strain –void ratio relation of each element –2D (Infinitesimal deformation theory, OCR=10).

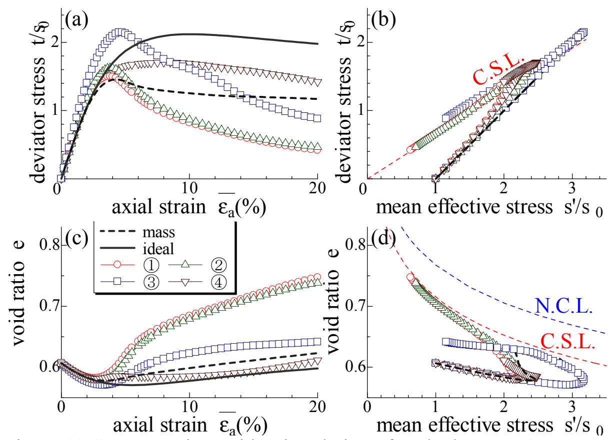

Figure 12 Stress- strain –void ratio relation of each element –2D (Finite deformation theory, OCR=10).

respect to the strain theory, the results were almost the same for both the finite deformation and infinitesimal deformation theories for both normally and over consolidated clay.

Figures 7 and 8 show the distributions of deviator strain for different values of the axial strain, after the average behavior started to deviate from the ideal behavior. The displacement pattern shows the top face moving to left-hand side for both conditions. In the case of normally consolidated clay, the localized deviator strains distributed over a wider region and the shear band cannot be seen as clearly as in the case of over consolidated clay with infinitesimal deformation theory. With finite deformation theory, the deviator strains occur locally for both normally and over consolidated clays.

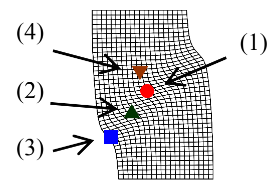

Figures 9 and 10 show the distributions of volumetric strain for NC and OC clays, respectively. For normally consolidated clay, large volumetric contraction is observed over most of the specimen except at the upper left and the lower right parts (Figure 9). This is because normally consolidated clays show negative dilatancy. On the other hand, for over consolidated clay the regions of concentrated shear stresses and volumetric expansion are almost the same. Although the elements in the shear band expand uniformly for finite deformation theory, the elements in the edge of the shear

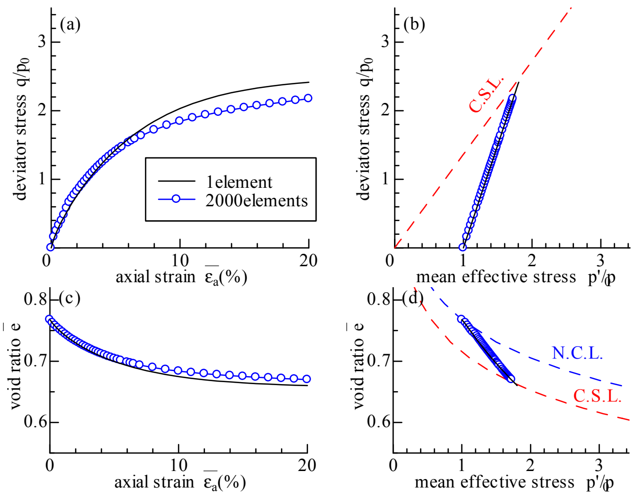

Figure 13. Stress- strain –void ratio relation as amass –3D (OCR=1).

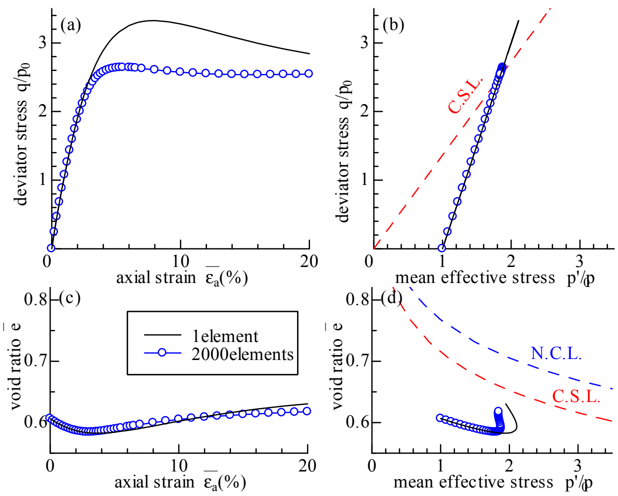

Figure 14. Stress- strain –void ratio relation as amass –3D (OCR=10).

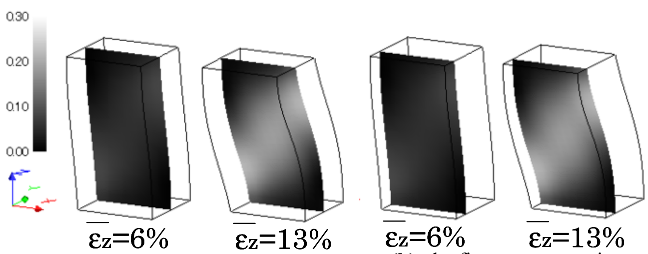

(a) the middle section **(b)** the first quarter section

Figure 15. Distributions of deviator strain –3D(OCR=1).

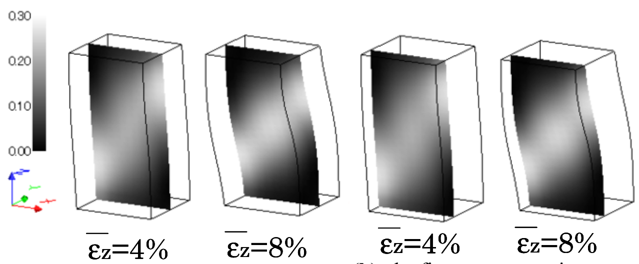

(a) the middle section **(b)** the first quarter section

Figure 16. Distributions of deviator strain –3D(OCR=10).

band expand more than the elements in the centre of the shear band for infinitesimal deformation theory.

The mechanism of development of the shear band is examined using the results for the over consolidated clay, for which the shear band is more clear. Four elements in different positions inside the specimen are analyzed: (1) element in the centre of specimen, (2) in the shear band, (3) in the end of the shear band, (4) near the shear band. The stress-strain relation of each element is shown in Figure 11 (infinitesimal deformation theory) and Figure 12 (finite deformation theory). Element (1) in the centre of the specimen reaches peak strength and then softens earlier than the others. Elements (2) and (3) show the same tendency as element (1). Therefore, the element at the center of the specimen softens first and acts as a trigger. After that the strain softening domain expands towards the boarders of the specimen, forming a shear band.

Figures 13 and 14 show the result of the 3D finite element analysis based on infinitesimal deformation theory. From the stress-strain relation in diagram (a) it can be noticed that the average curve shows some hardening and then deviates from the ideal behavior after some stage of shearing, similar to what was observed under plane strain conditions. The change of void ratio is almost same as that of the ideal behavior. The same general tendency is observed for the 3D and plane strain simulations, with the average curve failing earlier and reaching lower peak stresses than those computed for the ideal curve at a single point.

Figures 15 and 16 show the distributions of deviator strain for normally and over consolidated clays. Diagram (a) shows the distribution of deviator strain at the middle section of the specimen, and diagram (b) shows the same at a section near the lateral face in the first quarter section of the specimen. An inclined region where deviator strains are concentrated can be seen in these figures, similarly to what was observed under plane strain conditions. However, deviator strains are not as localized as in the plane strain case and a shear band is not clearly formed. Comparing Figures 15(a) and 15(b), or Figures 16(a) and 16(b), it is seen that the distribution of deviator strain is almost the same in every section of the specimen.

5 CONCLUSIONS

Finite element analysis can simulate the formation of the shear band, which is observed in actual laboratory tests, not only using finite deformation theory, but also using infinitesimal deformation theory. Moreover, the generation of the shear band can be explained with simple drained analyses without using soil-water coupled effects. By comparing the results obtained with 2D and 3D analyses, it was observed that the localization is more likely to be produced under two dimensional conditions. Finally, it is concluded that the isotropic hardening elastoplastic model (subloading t_{ij} model) is a useful tool to study localization problems with finite element analysis.

REFERENCES

Asaoka, A., Nakano, M. & Noda, T. 1997. Soil-water coupled behavior of heavily overconsolidated clay near/at critical state, *Soils & Foundations* 37(1):13-28.

Asaoka, A. & Noda, T. 1995. Imperfection-sensitive bifurcation of Cam-clay under plane strain compression with undrained boundary, *Soils & Foundations* :35(1):83-100.

Hashiguchi, K. 1980. Constitutive equation of elastoplastic materials with elasto-plastic transition, *J. Appl, Mech., ASME*, 102(2): 266-272.

Hinokio, M., Nakai, T. and Aramaki, K. 2002. Numerical analysis using *subloading* t_{ij} *model* for localized deformation of clay based on small deformation theory, *pro.of Iws-Calgary*: 75-82.

Nakai, T. and Hinokio, M. 2004. A simple elastoplastic model for normally and over consolidated soils with unified material parameters, *Soils & Foundations*: 44(2): 53-70.

Nakai, T. & Matsuoka, H. 1986. A generalized elastoplastic constitutive model for clay in three-dimensional stresses, *Soils and Foundations*. :26(3): 81-98

Oka, F., Adachi, T. &Yashima, A. 1995. A strain localization analysis using a viscoplastic softening model for clay, *Int. J. of Plasticity*, 11(5): 523-545.

Yatomi, C., Yashima, A., Iizuka, A. & Sano, I. 1989. General theory of shear bands formulation by a non-coaxial Cam-clay mode, *Soils & Foundations*: 29(3): 41-53.